Uplift and strength evolution of passive margins inferred from 2D conductive modelling

M. Leroy, Frédéric Gueydan, Olivier Dauteuil

Geophys. J. Int. (2008) **172,** 464–476 doi: 10.1111/j.1365-246X.2007.03566.x

Uplift and strength evolution of passive margins inferred from 2-D conductive modelling

Marie Leroy, Frédéric Gueydan and Olivier Dauteuil

Géosciences Rennes (UMR CNRS 6118*), Université de Rennes* 1, 35042 *Rennes Cedex, France. E-mail: frederic.gueydan@univ-rennes1.fr*

Accepted 2007 July 27. Received 2007 May 22; in original form 2005 October 13

SUMMARY

Post-breakup vertical motions of passive margins are seen here as a result of the post-rift 2-D thermal evolution. A 2-D finite element numerical model is performed to evaluate both the vertical and horizontal conduction that drive the thermal evolution of continental passive margins, from breakup to post-breakup states. Initial temperature configurations corresponding to non-volcanic and volcanic margins are tested, and lead to different thermal evolution of the lithosphere. For both margins, a thermal thickening is observed in the stretched lithosphere, whereas the unstretched lithosphere undergoes first (0–80 Ma) a thermal thinning and secondly (after 80 Ma) a thermal thickening. In comparison with non-volcanic margins, volcanic margins show a slower thermal thickening and a greater thermal thinning in stretched and unstretched lithosphere, respectively. The variations with time of lithosphere thickness are then translated into isostatic vertical movements and reveal 'seaward' thermal induced subsidence and 'landward' thermal induced uplift. The estimated uplift reaches up to 250 m in volcanic margins and 120 m in non-volcanic margins. The modelled timing and amount of uplift in both margins are consistent with present-day topography of volcanic passive margins that stand two to three times higher than non-volcanic margins. Using these thermal models, we finally show that the 2-D strength of the margins drastically evolves with time from a seeward dominant strength (0–80 Ma) toward a landward dominant strength (time larger than 80 Ma). These lateral strength evolution could have strong effect on the flexural response of the margin through time.

Key words: Numerical solutions; Heat flow; Rheology: crust and lithosphere.

1 INTRODUCTION

Passive margins are commonly seen as stable geodynamic features, only affected by subsidence, driven first by tectonic and then by thermal re-adjustments (McKenzie 1978). The inland topography is assumed to be inherited from rifting and evolves with erosion and isostatic response. However, many margins display a continental part with a high topography that is likely related to post-breakup vertical motions. Significant post-rifting uplift has indeed been recognized in northwestern Europe (Stuevold & Eldholm 1996; Japsen & Chalmers 2000), in West Africa (Partridge & Maud 1987; Burke 1996), southeast Brazil (Cobbold *et al.* 2001; Saenz *et al.* 2003) and India (Gunnel & Fleitout 2000). For example, in South Africa, the uplift amount reached 900 m in Pliocene (Partridge & Maud 1987). These uplift occurrences raise a major problem that is to constrain the mechanisms controlling the post-breakup rejuvenation of topography associated to the passive margin uplift.

This topography rejuvenation has to be differentiated from the topography inherited from the rifting of passive margins. Rifting results in a syn-rift topography caused by the rift flanks uplift that can be added to the pre-rift inherited topography. Isostatic adjustment, lithosphere flexure, depth-dependant extension, deep crustal flow and thermal expansion due to small-scale convection are commonly advocated to explain rift flank uplift (Beaumont *et al.* 1982; Buck 1986; Rowley & Sahagian 1986; Braun & Beaumont 1989; Weissel & Karner 1989; Kruse *et al.* 1991; Chéry *et al.* 1992; Hopper & Buck 1996, 1998). All these processes occur during rifting and thus could not explain the recognized post-rift uplift. The mechanisms responsible for post-breakup rift uplift remain poorly understood and are matter of debate. Glacial rebound, lithospheric flexure due to erosion and sedimentation, mantle plume effects and regional compression have been proposed to explain post-rift uplift (Gilchrist & Summerfield 1990; Nyblade & Robinson 1994; Stuevold & Eldholm 1996; Japsen & Chalmers 2000; Cobbold *et al.* 2001). For example, tectonic horizontal forces such as ridge-push or far-field tectonic stresses may trigger margins reactivations in compression and thus induce uplift (Cloetingh *et al.* 1990; Ransome & de Wit 1992; Doré & Lundin 1996; Boldreel & Andersen 1998; Hudec & Jackson 2002; Mosar *et al.* 2002). The uplift could also be enhanced after the breakup by subcontinental hotspots, like in the south of Africa where a significant uplift has been attributed

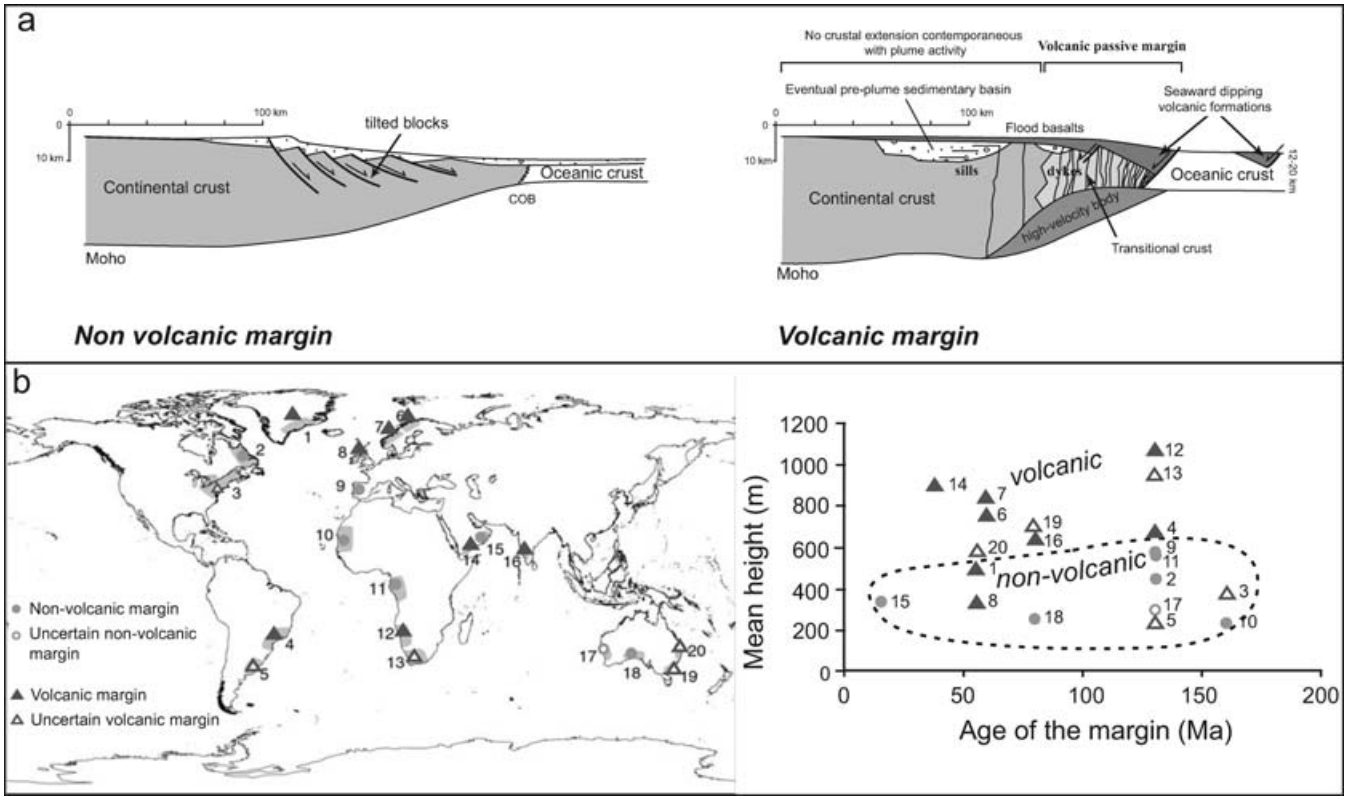

Figure 1. (a) Crustal geometry and principal features of non-volcanic (modified from Boillot 1979) and volcanic passive margins (modified from Geoffroy 2001). Volcanic margins are marked by intrusion and extrusion of large volumes of magma, sills and dykes, and by seaward dipping layers of sediments and volcanics; (b) Mean height of 20 volcanic and non-volcanic passive margins plotted as a function of the age of the margins. Characteristics of the 20 passive margins are displayed in Table 1. The type of margin is from Coffin & Eldholm (1992): Non-volcanic margins are plotted with black dots (full when the non-volcanic aspect at breakup time is certain, empty when uncertain) and Volcanic margins are displayed with black triangles (full when the volcanic aspect of the province at breakup time is certain, empty when the volcanic association with breakup time is uncertain).

to the 'African Superswell' (Nyblade & Robinson 1994; Gurnis *et al.* 2000). The edge-driven convection induced by sharp lithosphere topography, could also promote the driven forces necessary for the margins uplift (Buck 1986; King & Anderson 1998; Boutilier & Keen 1999; Huismans *et al.* 2001). This small-scale convection was used to study the convective destabilization of lithosphere cratonic roots, with a high and steep lithosphere thickness difference. For passive margins, the lithosphere thinning is much more gradual and edge-driven convection is probably less favourable.

The origin of post-breakup uplift is still controversial and associated processes remain poorly understood. We propose here to study the impact of the steep lateral thermal gradient produced by rifting on the 2-D thermal evolution of the margins and thus on the lateral isostatic evolution of the margin. This thermal re-adjustment could have a major impact because rifted continental margins may be contemporaneous to magmatic event yielding to volcanic or non-volcanic margin according to the thickness of igneous crust on the margin, and to the presence of a hotspot during breakup. Around 30 per cent of passive margins are said to be non-volcanic (Northwestern Africa margins, for example), and 70 per cent volcanic (e.g. Greenland, Norway, Namibia and Brazil margins, Ruppel 1995). In addition to the structural difference of these two margin types described by several authors (Boillot 1979; White & McKenzie 1989; Banda *et al.* 1993; Gladczenko *et al.* 1997; Price *et al.* 1997; Brun 1999; Eldholm *et al.* 2000; Jackson *et al.* 2000) and displayed on Fig. 1(a), these margins have distinct initial 2-D thermal state. Volcanic margins are indeed marked by warmer geotherms than that of non-volcanic margins and are associated with voluminous intrusive and extrusive volcanic activity (White & McKenzie 1989; Eldholm 1991; Skogseid *et al.* 1992; Gladczenko *et al.* 1997; Price *et al.* 1997; Eldholm *et al.* 2000; Jackson *et al.* 2000). Moreover, positive temperatures anomalies of 100–200 °C are generated by mantle plumes beneath the lithosphere in the underlying asthenosphere (White & McKenzie 1989). As well as the subsidence is strongly controlled by the thermal re-adjustment of the lithosphere (McKenzie 1978), that is, the initial thermal state of the margin and the heat flow at the lithosphere base, this paper aims to constrain the thermal effects on post breakup margin uplift in 2-D.

This hypothesis of margin uplift related to 2-D post-breakup thermal adjustment is strengthened by the present-day margin topography that is higher for volcanic margin (Fig. 1b). The mean height of 20 margins were computed from the Digital Elevation Model ETOPO 30 (full data in Table 1) and plotted as a function of the margin age, estimated from the UNESCO geological map. The topography of volcanic margins is higher (∼700 m) than that of non-volcanic margins (∼300–350 m). Assuming that this topography images the uplift history of the margins, this feature would suggest that volcanic margins have undergone higher uplift since breakup (two to three times higher), which may be the consequence of its warmer breakup 2-D thermal state. As discussed above, the present-day margin topography however results from the sum of several processes like inherited rifting topography, post-rift erosion rate, flexural deformation of margins and 2-D post-breakup thermal re-adjustment.

Table 1. Description of the 20 passive margins displayed on Fig. 1: localization, drifting age, type of margin [volcanic (V) or non-volcanic (NV) from Coffin & Eldholm 1992].

Margin	Country	Mean height (m)	Approximated age (Ma)	Type of margin volcanic (V) non volcanic (NV)
1	Greenland	488	55	V
2	Canada	445	130	NV
3	USA	372	160	V?
4	Brazil	674	130	V
5	Uruguay/Argentina	225	130	V?
6	Norway	750	60	V
7	Norway	836	60	V
8	British Isles	326	55	V
9	Spain/Portugal	558	130	NV
10	Senegal/Mauritania	234	160	NV
11	Gabon	556	130	NV
12	Namibia	1064	130	V
13	South Africa	951	130	V?
14	Yemen	886	40	V
15	Oman	360	17	NV
16	India	641	80	V
17	Australia	295	130	NV?
18	Australia	252	80	NV
19	Australia	700	80	V?
20	Australia	583	55	V?

Question marks stand for uncertainties for the type of margins. For the Greenland margin ($n\,^{\circ}1$), we have subtracted from the mean elevation calculated, the 2000 m corresponding to the supposed icecap thickness (see website: http://www.geocities.com/Yosemite/4466/mapintro.html).

Thermal evolution of the oceanic part of the margins has been widely studied (see for example, Parsons & Sclater 1977; Karner 1985; Stein & Stein 1992), but the continental lithosphere thermal evolution is less constrained. The most famous post-rift thermal model for passive margins is the 1-D conductive model proposed by McKenzie (1978), which computed post-rift subsidence in the stretched part of the continental margin. This model predicts the tectonic and thermal subsidence and the timescale of each process. The horizontal variations of temperature with time along the margin (from stretched to unstretched continental lithosphere), and the related vertical motions in the unstretched part of the margin due to isostatic compensation were however not discussed by McKenzie and are the objective of the present paper. Several others models have been performed on the 2-D thermal evolution of margin (Cochran 1983; Gadd & Scrutton 1997; Vagnes 1997; Hansen & Nielsen 2002) and show that lateral heat conduction has a significant effect on the basin subsidence and margin uplift histories. Cochran (1983) suggests for example that uplift could be generated by thermal expansion in areas surrounding basins; but with small amplitude ($<$50 m) and small duration (few Ma after the end of rifting). From these considerations, we focus this study on the role of initial thermal state of the lithosphere in post-rift continental uplift.

First, we describe the 2-D numerical model that computes the temperature evolution of the lithosphere with time, from an initial thermal state. For sake of simplicity, convection has been disregarded in this study. We chose to focus this study on the role of 2-D conduction in lithosphere thinning and thickening, and the related vertical motions. Different initial thermal configurations, corresponding to non-volcanic and volcanic margins, are tested and analysed in term of thermal buoyancy forces and surface effects. Our results are then tentatively compared with natural observations of passive margins topography that provide indirect images of the uplift. Finally, the strength evolution of margins is discussed.

2 2-D THERMAL MODEL

We have performed a 2-D thermal numerical model at lithosphere scale to compute the isotherm re-adjustment driven by 2-D conduction of the two types of passive margins after the stretching event. This re-adjustment depends on the initial thermal configuration, and therefore, on the margin geometry.

2.1 Initial 2-D thermal state

This modelling assumes that the initial thermal state is that of the drifting stage of a passive margin, when the oceanic crust is just formed (Fig. 2). At this time, the continental crust is highly thinned and stretched. The whole lithosphere is getting thinner towards the ocean/continent boundary, as expressed by the 1200 °C isotherm defining the base of the lithosphere (Fig. 2, stage 1). The 2-D thermal modelling will thus capture the isotherm re-adjustment from this initial thermal state towards the thermal equilibrium of the margin (Fig. 2, stage 2). During the thermal re-adjustment, the continental crust is assumed to keep the stretched shape acquired at the beginning of the drifting stage. This assumption is in agreement with many seismic profiles that show a strong Moho deflexion in present days below passive margins (Mohriak & Dewey 1987; Gladczenko *et al.* 1997; Bauer *et al.* 2000; Eldholm *et al.* 2000). The 2-D modelled box is 600 km long and 150 km thick and consists of a continental lithosphere of thickness H_L and a portion of the asthenosphere (Fig. 2). The oceanic lithosphere has not been modelled, since our main objective is to study the thermal evolution of the unstretched continental domain of the passive margins, and its uplift. The studied structure starts a few kilometres after the ocean/continent boundary, as sketched in shaded rectangle on Fig. 2. The crustal thickness is set to 30 km in the unstretched continental lithosphere and decreases in the stretched lithosphere, near the ocean/continent boundary, to reach $30/\beta$ km, β being the stretching factor.

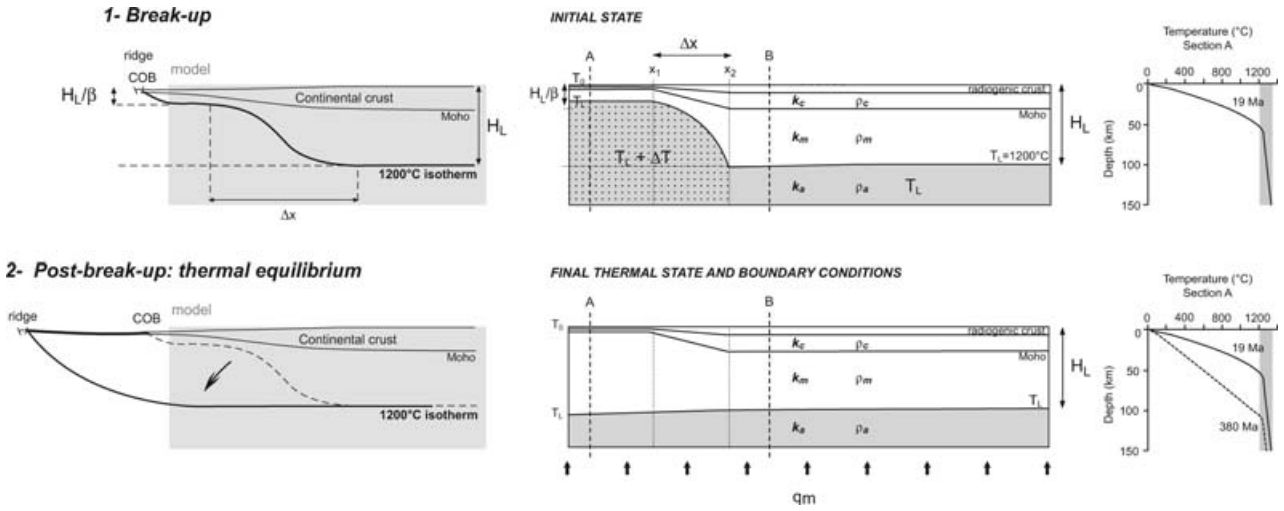

Figure 2. Geometry and thermal structure of a passive margin in nature (left-hand side) and in the numerical model (right-hand side), (1) at the end of continental breakup (initial state) and (2) tens of Ma after drifting, when the lithosphere is thermally re-equilibrated (stable thermal state). The 1200 °C isotherm defines the lithosphere bottom. Its shape under continental part is defined from the initial thermal state, by the stretching factor β and value Δx. The asthenosphere temperature beneath the stretched part is set to 1200 °C + ΔT (ΔT varying between 0 and 200 °C for different model set up).

The initial thermal state was defined as follows. First, a 2-D steady state is defined to account for a 100 km thick lithosphere at thermal equilibrium in the stable margin (right of the model).

For this steady state, the temperature $T(x, z)$ in the crust is:

$$\underline{\text{Radiogenic crust } [z < H_{\text{RC}}(x)]:}$$
$$T(x,z) = -\frac{r}{2k_c}z^2 + \left(\frac{q_m}{k_c} + \frac{r}{k_c}H_{\text{RC}}(x)\right)z + T_o; \quad (1)$$

$$\underline{\text{Non} - \text{radiogenic crust } [H_{\text{RC}}(x) < z < H_C(x)]:}$$
$$T(x,z) = \frac{q_m}{k_c}z + \frac{r}{2k_c}H_{\text{RC}}(x)^2 + T_0, \quad (2)$$

where r, k_c, q_m and T_0 are the radiogenic heat production [which occurred over a thickness $H_{\text{RC}}(x)$], the crust conduction, the basal heat flux and the surface temperature set to 300 °K, respectively. x and y are the horizontal and vertical coordinates, respectively. x is increasing toward the right and y is increasing downward. The thickness of the crust $H_c(x)$ and the radiogenic crust $H_{\text{RC}}(x)$ are two functions of the horizontal coordinate x, which are defined as follows. The radiogenic crustal thickness is set to the third of the crustal thickness: $H_{\text{RC}}(x) = H_C(x)/3$. In the unstretched part of the lithosphere ($x > x_2$, Fig. 2), the crustal thickness is $H_{\text{co}} = 30$ km (Table 1), while in the stretched part of the lithosphere ($x < x_1$), $H_{\text{c}} = H_{\text{co}}/\beta$. For $x_1 < x < x_2$, a linear evolution of the crustal thickness is imposed.

In the mantle, the temperatures are defined by:

$$\underline{\text{Lithosphere mantle } [z > H_C(x)]:}$$
$$T(x,z) = \frac{q_m}{k_m}[z - H_C(x)] + T_M(x); \quad (3)$$
$$\text{with } T_M(x) = \frac{q_m}{k_c}Hc(x) + \frac{r}{2k_c}H_{RC}(x)^2 + T_0,$$

where k_m and k_c are the mantle and crust conductions, respectively. $T_M(x)$ is the Moho temperature. The thickness of the lithosphere $H_L(x)$ could be derived from eq. (3) since at $z = H_L(x)$, the lithosphere temperature is $T_L = 1200$ °C (Table 1):

$$H_L(x) = \frac{k_m}{q_m}[T_L - T_M(x)] + H_C(x). \quad (4)$$

Finally, in the asthenosphere $[z > H_L(x)]$, the temperature is set to T_L for $x > x_2$ and to $T_L + \Delta T$ under the stretched lithosphere ($x < x_2$, Fig. 2), in order to model the hot condition of volcanic margins asthenosphere. We have chosen to consider this temperature anomaly as a localized feature in the mantle below the stretched lithosphere because this thermal anomaly likely induced crustal underplating and sills and dykes emplacement only in the vicinity of the stretched crust (Fig. 1a). The value of this positive thermal anomaly ΔT will be systematically varied in this study. We consider here 200 °C as the maximum value for the temperature anomaly in the mantle (White & McKenzie 1989).

From this 2-D steady state (eqs 1–3), the temperature profiles are modified to account for the stretching factor β. For $x < x_1$, the base of the lithosphere is changed from $H_L(x)$, eq. (4), to $H_L(x)/\beta$ (Fig. 2). For $x > x_2$, the thickness of the lithosphere remains unchanged to $H_L(x)$ and for $x_1 < x < x_2$, a linear interpolation of the lithosphere thickness is imposed. The lateral variation of the initial lithosphere thickness over the passive margin is, therefore, controlled by the stretching factor β over the horizontal distance $\Delta x = x_2 - x_1$ (Fig. 2). These two parameters (β and Δx) will be used to characterize the initial thermal state. The thickness interpolation results in the initial state geometry displayed on Fig. 2. Note that the particular unsmooth shape of the lithosphere at x_2 is a meshing effect in this area of the model but has no incidence on the thermal evolution and on the model results. As well, in our thermal modelling, the zone where the crust gets thinner is modelled with the same length (Δx) for volcanic and non-volcanic margins, although it appears to be shorter in volcanic margins (Fig. 1a). This approximation may not influence significantly the thermal structure, but its role on the thermal evolution could however be studied in future development of this model.

2.2 Governing equations and boundary conditions

The heat equation solved is the 2-D formulation of the time dependant heat conduction, which reads:

$$\rho\, C\frac{\partial T}{\partial t} - \left(k\frac{\partial^2 T}{\partial z^2} + k\frac{\partial^2 T}{\partial x^2}\right) = r, \quad (5)$$

where ρ and C are the material density and the heat capacity, respectively. Values of these parameters for the crust and the mantle can be found in Table 2. The radiogenic heat production is fixed

Table 2. Thermal parameters used for the 2-D modelling and rheological parameters used to estimate the margin strength.

Symbol	Parameter	Value
r	Radiogenic heat production	1.5 μW m^{-3}
kc	Conduction of the crust	2.1 W m^{-1} K^{-1}
km	Conduction of the mantle	3.0 W m^{-1} K^{-1}
ka	Conduction of the asthenosphere	30 W m^{-1} K^{-1}
q_m	Basal heat flux	30 mW m^{-2}
ρ	Material density	
	Crust	2800 kg m^{-3}
	Mantle	3300 kg m^{-3}
	Asthenosphere	3300 kg m^{-3}
C	Material capacity	1000 J kg^{-1} K^{-1} for crust and mantle
μ	Friction coefficient	0.6
A	Pre-exponential constant (MPa^{-n} s^{-1})	Crust: 3.2 $\times$ 10^{-4}
		Mantle: 3.9 $\times$ 10^{3}
Q	Activation energy (kJ mol^{-1})	Crust: 154
		Mantle: 430
n	Stress exponent	Crust: 2.3
		Mantle: 4.0

Ductile creep law is $\dot{\varepsilon} = A \exp(\frac{-Q}{RT})\tau^n$, where $\dot{\varepsilon}$, T and τ is the strain rate (s^{-1}), the temperature (in °K) and the shear stress (strength, in MPa). A, Q and n are material constant and are the pre-exponential constant (MPa^{-n} s^{-1}), the activation energy (kJ mol^{-1}) and the stress exponent. Values of these parameters are for Wet Quartz for the crust (Ranalli 1995) and dry olivine for the mantle (Karato & Wu 1993).

to zero for depths greater than $H_{RC}(x)$. The boundary conditions are as follows. The surface temperature is set to T_0, and the basal heat flux q_m to 30 mW m^{-2} so that the equilibrium lithosphere thickness is around 100 km Note that since the crustal thickness and the radiogenic crustal thickness varies with the horizontal distance, the equilibrium lithosphere thickness also varies along the margin. The thinner the crust is, the thicker is the equilibrium lithosphere thickness (eq. 4), with however slight variation in lithosphere thickness. The asthenosphere is modelled with a high conduction k_a that is 10 times larger than that of the lithospheric mantle ($k_a = 10\ k_m$), in order to obtain a quasi adiabatic temperature profile which well reproduce convective type geotherm in the asthenosphere (Fig. 2).

The time evolution of heat conduction is solved by numerical means, using the finite elements approximation for the spatial discretization and the finite-difference method for the time discretization, using the code SARPP (Structural Analysis and Rock Physics Program 2003). The lithosphere is discretized into 60 $\times$ 60–9 nodded Lagrangian Elements. This 2-D numerical model is a pure conductive model and, therefore, cannot predict any deformation (e.g. fault, buckling and flexure) leading to surface deformation. The vertical motion of the surface induced by thermal re-adjustment will be however estimated from the variation of lithosphere–asthenosphere boundary through time, using the principal of local isostasy in the terms of Airy.

3 NUMERICAL RESULTS

The differences in the initial thermal state are modelled by using different values of stretching (β), of initial stretched length (Δx) and of mantle thermal anomaly (ΔT). First we have chosen to present the results of two models differing in ΔT values and with similar β and Δx set to 6 and 100 km, respectively. Models with $\Delta T = 0$ °C simulate the thermal state of non-volcanic margins, while models with $\Delta T = 200$ °C are chosen to represent the volcanic passive margins as it corresponds to the maximum temperature anomaly in that case (White & Mckenzie 1999). The role of β and Δx will be explored later in a parametric study.

3.1 Thermal 2-D evolution of the passive margins

Fig. 3 shows the time evolution of the 2-D thermal states within the passive margins at five different times after the breakup (0, 20, 60, 120 and 180 Ma).

3.1.1 $\Delta T = 0$ °C

At the end of the breakup (time = 0 Ma), the lithosphere base defined by the 1200 °C isotherm deepens from about 17 km beneath the thinned crust (left of the model), towards 100 km deep under non-thinned continental crust (right of the model).

After the breakup, the thinned lithosphere cools as illustrated by the progressive deepening of the isotherms. The 1200 °C isotherm tends to reach an horizontal thermal state at around 100 km deep, in agreement with the heat flux q_m of 30 mW m^{-2} and eqs (2) and (3). This equilibrium state is nearly obtained after 180 Ma. In the right part of the model (unstretched lithosphere), we observe in the vicinity of the break in slope of the margin, a little thermal thinning, characterized by the upward migration of isotherms in the model (times 20, 60 and 120 Ma). The lateral extension of this phenomenon increases with time as shown in Fig. 3 with the black arrows. The isotherms in this part of the model should not have changed, because the imposed heat flux, the crustal thickness and the radiogenic crust thickness remain constant. This feature is thus explained by a lateral conductive heating, propagating from the stretched hotter part of the model towards the unstretched part of the margin. After 120 Ma, the isotherms deepen in this part of the model to reach progressively the stable thermal state. The part of the model located in the break in slope of the margin shows progressive isotherms deepening in accordance with the thermal re-adjustment expected.

3.1.2 $\Delta T = 200$ °C

The time evolution is rather similar to the previous model (Fig. 3). The differences are in the timing of the thermal equilibrium and the vertical and lateral extent of the heating.

In the unstretched lithosphere (right part of the model), the thinning of the lithosphere provoked by lateral heating is observed again at times 20, 60 and 120 Ma. However, the isotherms upward migration is more pronounced than in model $\Delta T = 0$ °C. After 20 Ma, the 1200 °C isotherm has undergone an upward migration of about 25 km in the vicinity of the crust break in slope. A greater lateral extent of the lithospheric thinning (120 km compared to around 45 km for $\Delta T = 0$ °C) is also observed for this stage (shown with black arrows). The lithosphere thickness is then progressively readjusted to its stable thickness of 100 km.

In summary, the 2-D conductive evolution of the passive margin after the breakup provokes a classical thermal cooling, resulting in a lithosphere thickening of the stretched margin as modelled in 1-D by McKenzie (1978), but it also leads to a thermal heating driven laterally from the hotter stretched margin towards the unstretched part of the margin. This lateral heating induces a thermal thinning of the lithosphere that is greater for the volcanic margins ($\Delta T =$ 200 °C); then migrates towards the continent and finally disappears progressively with time.

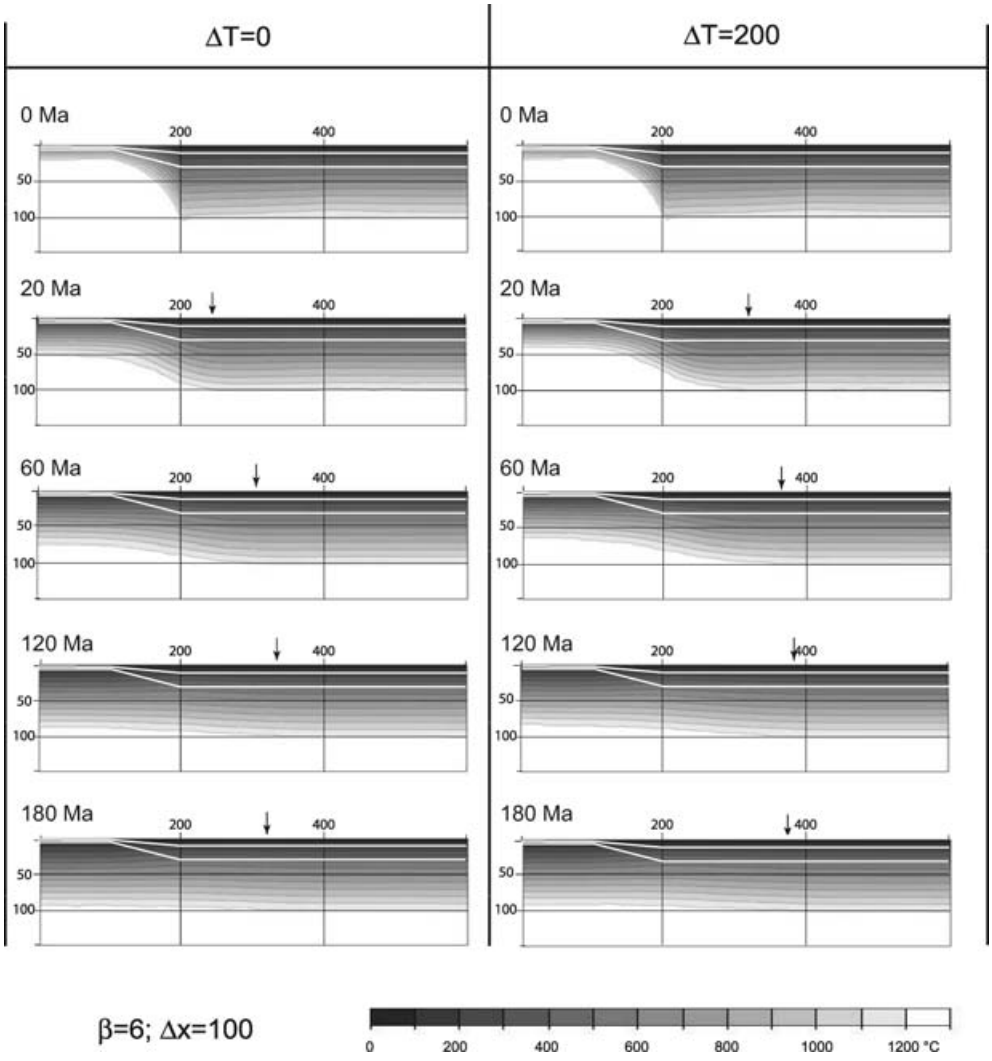

Figure 3. Thermal evolution of the lithosphere for two initial thermal configurations defined by $\Delta T = 0$ and 200 °C, whith $\beta = 6$ and $\Delta x = 100$ km. The evolution is displayed for 0, 20, 60, 120 and 180 Ma after breakup of the margin. The upper white line fixes the radiogenic/non-radiogenic boundary, while the lower white line defines the Moho depth. Twelve isotherms are plotted (one each 100 °C, from 0 to 1200 °C). The lateral progression of heating from the thinner part of the margin towards the unstretched margin is highlighted by the black arrows. The horizontal and vertical length scales are the same and values are given in kilometres. The base of the lithosphere in the stable unstretched continent is around 100 km.

3.2 Lithosphere thickness evolution and inferred vertical motion of the margin

The time evolution of the lithosphere thicknesses in two vertical cross-sections, located in the stretched and unstretched parts of the margins, are displayed on Fig. 4. The location of the two vertical cross-sections where the measurements have been done are reported on Fig. 2 (point A at $x = 25$ km for the stretched lithosphere and point B at $x = 250$ km for the unstretched lithosphere). The lithosphere thicknesses are inferred from the 2-D results of Fig. 3. From the lithosphere thickness evolution, the vertical motion of a point in the passive margin is estimated by classical isostatic equilibrium. Starting with a lithosphere thickness of H_{L_0} and a mean temperature of $T_L/2$, a given change in lithosphere thickness Δz yields a change in the topography Δh. Isostatic equilibrium yield:

$$\rho_0 g \left(1 - \alpha \tfrac{T_L}{2}\right) L_0 = \rho_0 g \left(1 - \alpha \tfrac{T_L}{2}\right) \times (L_0 + \Delta h - \Delta z) + \rho_0 g \Delta z, \quad (6)$$

where α is the coefficient of thermal expansion. The left-hand side term of the equation corresponds to the pressure at the base of the lithosphere of thickness Lo and of mean temperature $T_L/2$. The right-hand side term corresponds to the pressure at a depth of Δz below the new base of the lithosphere that has moved from L_0 to $L_0 - \Delta z$ with respect to the surface that is now at Δh.

This equation yields to the simple following relationship:

$$\Delta h = \alpha \frac{T_L}{2} \Delta z \quad (7)$$

with $\alpha = 3.28\ 10^{-5}\ ^\circ\mathrm{K}^{-1}$ and $T_L = 1200$ °C, we get:

$$\Delta h = 0.02\ \Delta z. \quad (8)$$

Thus a 10 km rise in the 1200 °C isotherm implies an uplift of 200 m.

Because the vertical motion of the margin Δh is directly related to the change in lithosphere thicknesses Δz, the time evolution of Δh and of the lithosphere thickness are exactly the same and are thus reported in the same plot with two distinct scales (Fig. 4). Thickening of lithosphere through time corresponds to subsidence while thinning is related to uplift.

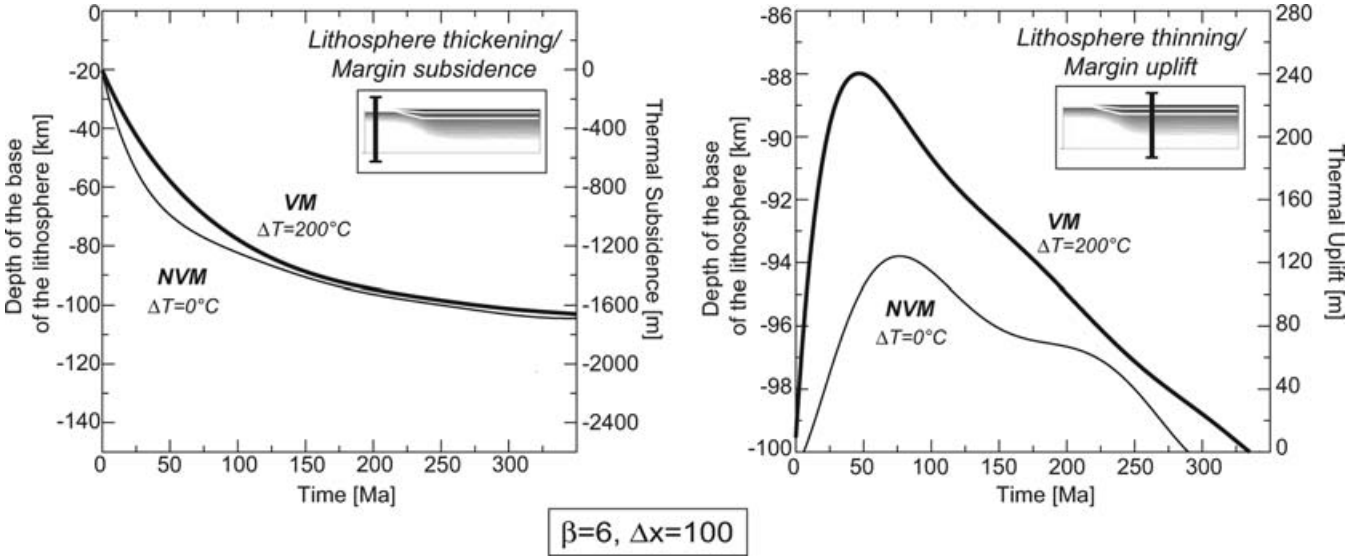

Figure 4. Lithosphere thickness evolution in two parts of the model (Sections A and B located in Fig. 2), during thermal re-adjustment and related subsidence/uplift. Lithosphere thickening/subsidence are observed in the stretched part of the margin (Section A in Fig. 2 and in inset), whereas lithosphere thinning/uplift occurs in early stages in the unstretched part (Section B in Fig. 2 and in inset).

In the stretched part of the model (Section A, left-hand side part of Fig. 4), the lithosphere thickness increases during the thermal re-adjustment for the two models ($\Delta T = 0$ and 200 °C). The thickening and subsequent margin subsidence is fast during the first 100 Ma (Fig. 4, left) and very similar for the two types of margins with a 80 km lithosphere thickening. This similarity is consistent with the findings of McKenzie (1978) that shows that the post breakup subsidence depends on β, which is the same for the two study models. A little delay in time is however observed between the two curves in early stages. The thickening/subsidence of non-volcanic margins ($\Delta T = 0$ °C) is more efficient between 0 and 100 Ma than that of the volcanic margin ($\Delta T = 200$ °C). This difference is explained by a larger lateral conduction in the volcanic margin, leading to a more pronounced lithosphere thinning in the unstretched part of the margin. The timing of the modelled subsidence is also consistent with the results of McKenzie (1978). The final amount of subsidence we obtain (1700 m) is however 500 m smaller than his estimation because we take into account the horizontal heat transfers but not the density variations in layers. The subsidence in volcanic models ($\Delta T = 200$ °C) is delayed compared to non-volcanic models ($\Delta T = 0$ °C) due to increase of lateral heating. The thermal anomaly ΔT seems, therefore, to control the subsidence rate.

In the unstretched margin (Section B, right-hand side part of Fig. 4), the lithosphere thickness decreases in the first tens of million years following the breakup, leading to passive margin uplift, and then increases to tend towards the stable thickness of 100 km. Large differences in lithosphere thinning and subsequent margin uplift are here observed between volcanic and non-volcanic margins. The lithosphere thickness of volcanic margin decreases from 100 to 88 km in 50 Ma (240 m of uplift) while the non-volcanic lithosphere thickness only attains 94 km (120 m of uplift) during 75 Ma. The maximum of thinning is obtained earlier for the volcanic margins ($\Delta T = 200$ °C) with larger values than for non-volcanic margins. The passive margin uplift is approximately twice larger for $\Delta T = 200$ °C than that for $\Delta T = 0$ °C (Fig. 5). The uplift ceases after ∼80 Ma in the non-volcanic margin (NVM) and after ∼40 Ma in the volcanic margin (VM). After this thinning stage, the lithosphere thickness increases in the two models and the stable lithosphere thickness of around 100 km is reached after 280 Ma for the non-volcanic margins, and after 320 Ma for the volcanic margins. Consequently, the margin topography progressively decreases as a consequence of the subsidence.

Two different stages thus characterize the margin topography in its unstretched part: first an uplift during the first 40–80 Ma after breakup due to lateral heating that is followed by a general subsidence that tends to progressively erase the margin topography. The maximum amount of lateral heating and consequently of lithosphere thinning and associated margin uplift are highly controlled by the thermal sublithospheric anomaly ΔT, and therefore, by the initial thermal state of the margin.

3.3 Maximum amount of uplift: parametric study

Fig. 5 displays the effect of the three parameters (ΔT, Δx and β) on the amount of maximal thermal uplift in metres computed in the unstretched margin. The thermal anomaly beneath the margin ΔT has the major influence, while Δx and β has little effect on margin uplift.

A decrease in β (from 6 to 4) leads to a smaller uplift in the unstretched lithosphere. For $\Delta x = 100$ and $\Delta T = 100$, the uplift is 50 m smaller for $\beta = 4$, than for $\beta = 6$. For $\beta = 4$, the initial thermal state of the stretched lithosphere is indeed colder and induces, therefore, smaller lateral heat transfers.

The effect of Δx, the horizontal distance over which stretching occurs, is the opposite of the effect of β: a decrease of Δx induces a slight increase in the amount of uplift by a few tens of metres. For a smaller Δx, the heat conducted laterally has a shorter distance to cover, between stretched and unstretched margin and has less time to dissipate. The uplift is thus greater and occurs earlier. In summary, the more β is high and Δx is small, the more the maximal uplift is great. Consequently, a higher initial slope of the margin leads to a greater uplift.

The effect of ΔT has been discussed in the previous sections: an increase in ΔT leads to a significant increase in the amount of uplift. The uplift for $\Delta T = 200$ °C is almost twice that for $\Delta T = 0$–100 °C, independently of the values of Δx and β (Fig. 5).

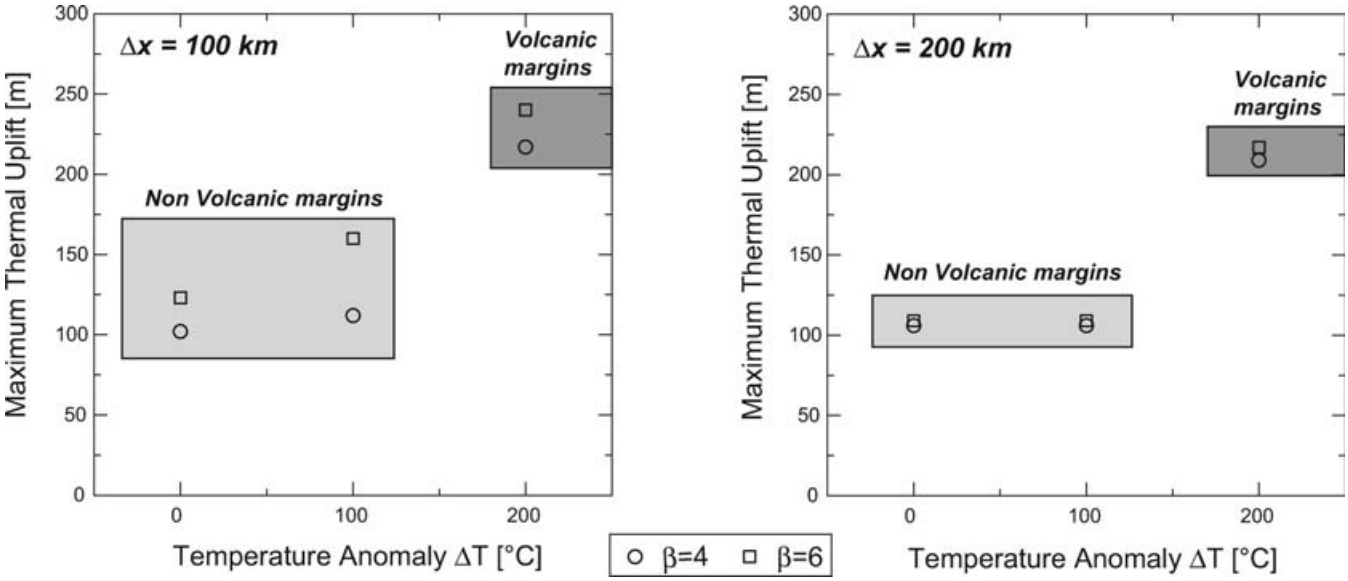

Figure 5. Maximal thermal uplift obtained in the unstretched margin (Section B) for various ΔT (0, 100 and 200 °C) and stretching factors ($\beta = 4$ and 6) with Δx set to 100 km (left-hand panel) or to 200 km (right-hand panel). The volcanic margins ($\Delta T > 100$ °C) are characterized by a greater thermal uplift than the non-volcanic margins ($\Delta T \leq 100$ °C).

If we consider that volcanic margins are characterized by a thermal anomaly higher than 100 °C in their stretched part (White & McKenzie 1989), these results suggest that the maximal thermal uplift in the case of volcanic margins ($\Delta T > 100$ °C) is two to three times higher than the non-volcanic margin ($\Delta T = 0$). These estimations assume a simple local isostasy response constant through the time. If a flexural term is integrated in a deformation pattern, the uplift will be controlled by the strength evolution of the stretched margin (see discussion below).

4 DISCUSSION

4.1 Comparison with natural examples of passive margins

The differences of uplift rates between the two types of margin are now tentatively compared with the present-day margin topography. We assume that the current topography (Fig. 1b) mostly results from post-rifting vertical movement. This assumption imposes that no significant relief existed before the continental breakup. This assumption is reasonable because all the margins do not display high topography like Argentina and Mauritania margins. A high margin topography is likely related to an important uplift since breakup, while a low topograpahy reflect a very small amount of post-breakup uplift. However, elastic flexure, erosion, sedimentation could modify the amount of uplift and subsidence during the post-breakup evolution of the margins and are here not taken into account. We will discuss these effects later in the paper.

The time evolution of the estimated thermal uplift in volcanic and non-volcanic margins is remarkably similar to the present-day topography of volcanic and non-volcanic margin (Fig. 6). In case of volcanic margins, numerical results indeed suggest that the relief will be maximum 50 Ma after the breakup and then linearly decreases with time. The observed present day-topography for volcanic margins of different ages (between 50 and 150 Ma) remarkably shows the decrease of the mean topography with increasing margin ages. Note that the Namibian and South-African margins have been neglected because of the location at the 'African Superswell' that increases considerably the topography (Nyblade & Robinson 1994; Gurnis *et al.* 2000). For non-volcanic margins, models suggest a low maximum uplift at 75 after the breakup and a smooth decrease of this uplift. This feature is consistent with a rather constant topography of Non-volcanic margins of distinct ages (between 20 and 160 Ma). The ratio of estimated maximum uplift between volcanic and non-volcanic margins is around 2–3, and is very close to the ratio of observed topography between these two types of margins. The topography of volcanic margins older than 150 Ma is very similar to that of non-volcanic margins, as suggested by the modelling results. These similarities thus strengthen the role of post-breakup thermal re-adjustments in generating the margin topography.

Another comparison between models and observation concerns the high denudation rate recognized in passive margins at early stages of their evolution. In Namibia, the margin formed 130 Ma ago and has undergone a high denudation period following the breakup, from 125 to 75 Ma (i.e. 5–55 Ma after the breakup, Gallagher & Brown 1999). In Brazil, high denudation rates are also recognized from 110 to 65 Ma, thus during the first 60 Ma after the breakup (Gallagher & Brown 1999). The high denudation rates recognized in early stages of the margins evolution could thus be related to the strong increase in the uplift rate during the first stage of thermal re-adjustment (0–60 Ma) predict by our modelling. It is interesting to note that the timing of higher uplift rate is compatible with the one predicts by the thermal re-adjustment, while tectonic models do not predict such a timing. This high uplift rate is synchronous to large sediment accumulation just after the drifting stage as shown by Emery & Uchupi (1984).

Finally, the subsidence is commonly assumed to be small in early stages of volcanic passive margins rifting (Clift 1996, 1997; Jackson *et al.* 2000; Skogseid 2001; Menzies *et al.* 2002). This feature is consistent with the slow thermal re-adjustment in early stages of volcanic passive margins modelled in this study (Fig. 6).

4.2 Strength and deformation of passive margins.

The relative small post-rift uplift induced by 2-D thermal evolution of the lithosphere is not sufficient to explain the present-day topography and the amount of uplift described on passive margins. Its

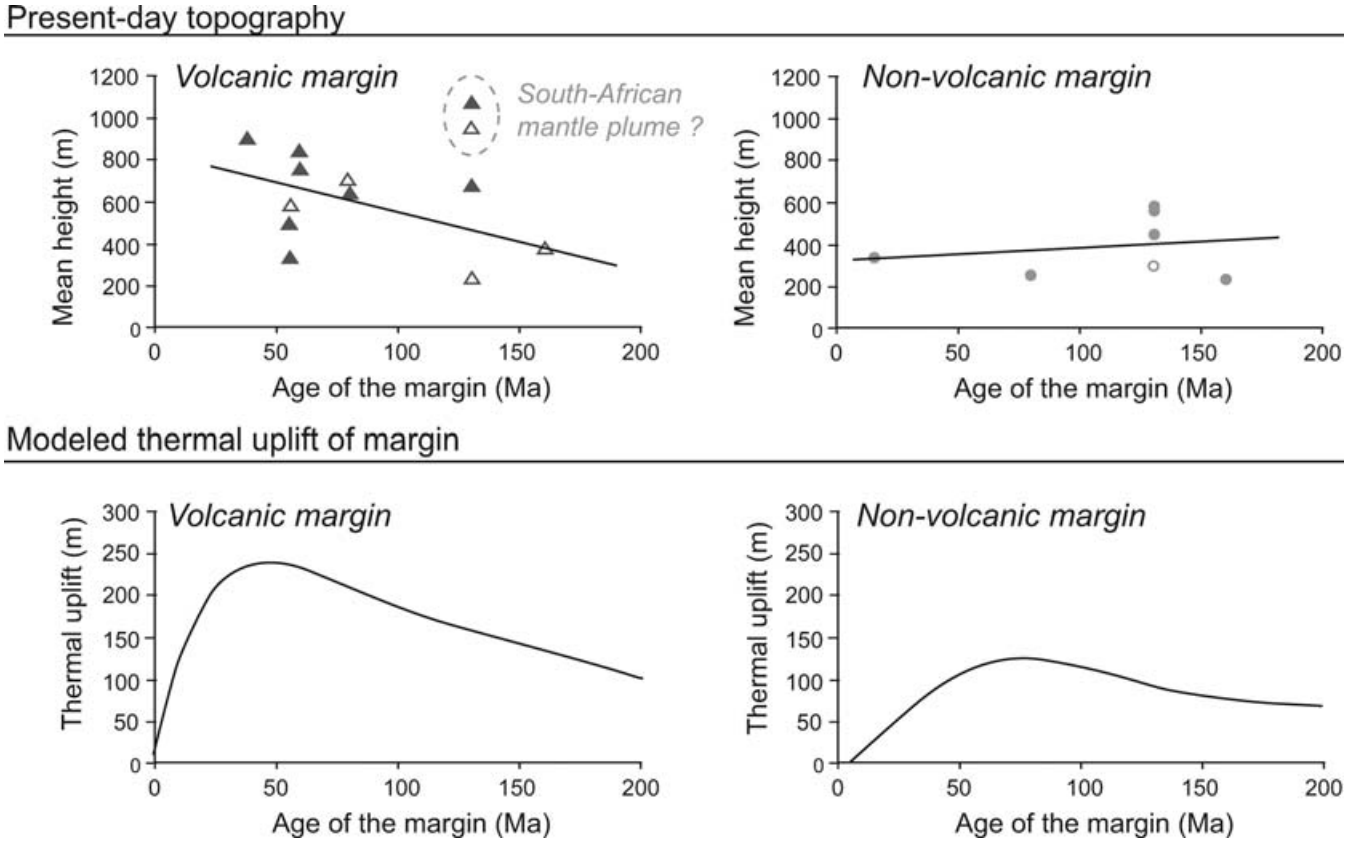

Figure 6. Mean height of volcanic and non-volcanic passive margins plotted as a function of the age of the margins compared to the thermal maximum uplift computed with our model ($\Delta x = 100$ km, $\beta = 6$ and $\Delta T = 0$ and 200 °C for non volcanic margin and volcanic margin, respectively). Except for two margins located in southern Africa and possibly submitted to the 'Superswell' effects, the topography evolution trend is similar with the thermal uplift computed in our models.

contribution may amount to 10–25 per cent of the whole uplift. This value shows that this process is not negligible. Others mechanisms should thus be evoked to explain higher amount of uplift, such as flexure response, small scale convection, tectonic stresses (far-field stress like ridge-push), lower crustal flow towards the rift flanks, and middle crustal flow towards the rift centre or mantle plumes (Gilchrist & Summerfield 1990; Gilchrist *et al.* 1994; Van Der Beek *et al.* 1995; Beaumont *et al.* 2000; Burov & Poliakov 2001; Huismans *et al.* 2001; Leroy *et al.* 2004). Our estimate of uplift and subsidence should thus be seen as a minimum estimate. Post-breakup flexure of the margin, triggered by horizontal far-field stresses and by loading of the stretched part (subsidence/sedimentation) and unloading of the unstretched part (erosion) of the margin, is the most evoked mechanisms to explain margin uplift (Watts & Ryan 1976; Bott 1996). To better constrain this effect on vertical motions, a modelling of 2-D flexure with an elastic thickness that varies in time and laterally along the margin because of transient thermal evolution is absolutely required. The interest of the present 2-D thermal modelling is to provide quantification of the strength and of the elastic thickness of the passive margin through time, which is crucial to accurately model the 2-D flexural response of the margin. From the 2-D thermal states of the margin, we computed the strength of the margin using brittle rheology and ductile flow laws described in Table 2. From these estimates, we have defined the continent/margin strength ratio that is the ratio of the overall strength of the unstretched part (computed as the depth integral of strength in profile B, Fig. 2) over the overall strength of the stretched part (computed in profile A, Fig. 2) (Fig. 7a). Similarly, from the 2-D thermal states, the elastic thickness of the margin has been estimated by the depth of the 450 °C isotherm (Pinet *et al.* 1991). As a consequence, the elastic thickness *Te* is a linear function of the Moho temperature and thus reflects the integrated strength of the continental lithosphere for a flexural response of long-term geological loads (Burov & Watts 2006). A decrease of the Moho temperature will induce an increase of *Te*. Using the 2-D thermal state of the margin through time, we have computed the ratio of *Te* in the unstretched continental part over *Te* in the stretched margin (Fig. 7b).

The time evolution of the continent/margin strength ratio is very similar for both margins (Fig. 7a). Immediately after the breakup, this ratio is around 600 for the two margins and then rapidly decreases. During the early stage of margins evolution, the unstretched part is much stronger than the stretched part. A strength ratio inversion occurs at 80 and 95 Ma for non-volcanic and volcanic margins, respectively. After this time, the strength ratio is almost stable, the stretched margin strength being slightly higher than the unstretched margin strength. The time evolution of the continent/margin elastic thickness ratio shows similar feature with different timing. Immediately after the breakup, the elastic thickness of the continent is 1.5–3 times larger than the elastic thickness of the margin, because of local heating in the rifted region. After 15–30 Ma, the elastic thickness of the margin becomes larger than the elastic thickness of the continent because of progressive and faster cooling of the rifted margin and because of a lower crustal thickness. The change of the elastic thickness ratio is faster than the change of the strength ratio because

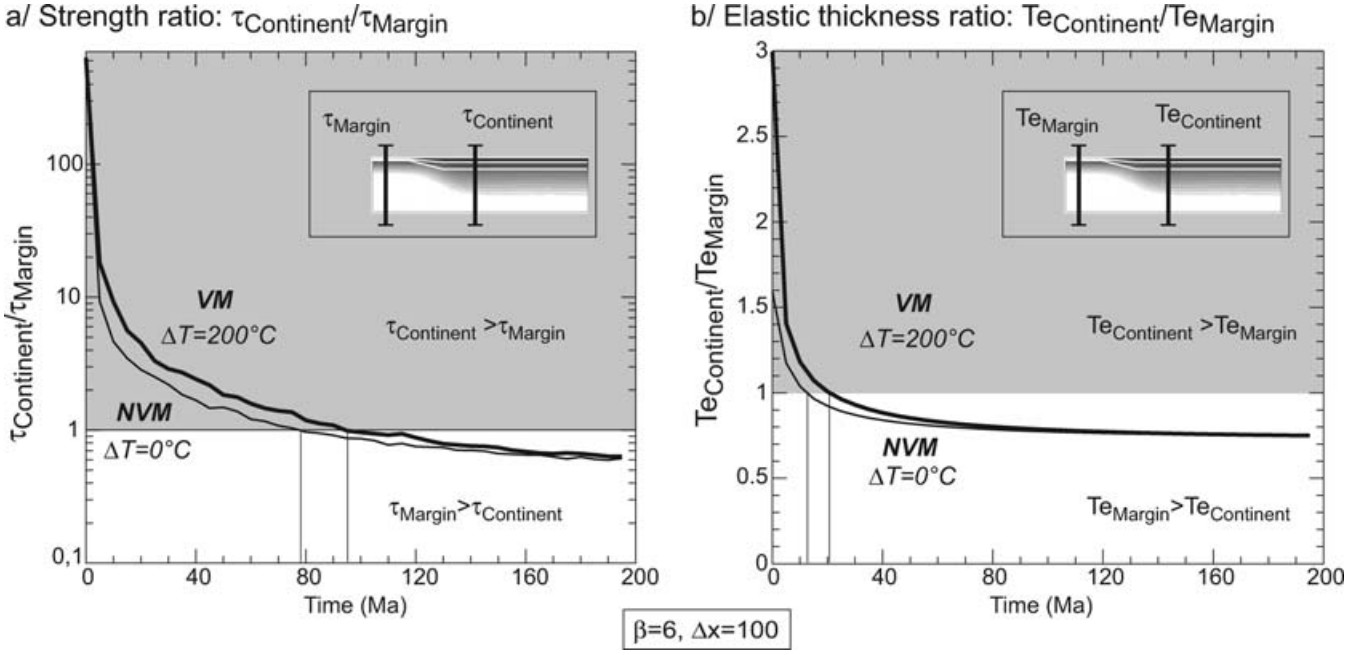

Figure 7. (a) Ratio of the strength of the unstretched part of the margin over the strength of the stretched part of the margin (continent-to-margin strength ratio) as a function of time. The integrated lithosphere strength is estimated from the 2-D thermal states, using rheological parameters given in Table 2 in the unstretched part (profile B of Fig. 2) and in the stretched part (profile A, Fig. 2). (b) Ratio of the elastic thickness of the unstretched part of the margin over the elastic thickness of the stretched part of the margin as a function of time.

elastic thickness is lineraly related to the Moho temperature while the integrated strength of the margin reflects crustal and mantle strength, that are non linearly dependant on the Moho temperature. From these results, the style of margin deformation should considerably vary through time. This strengthening of stretched margin controls a flexural response of the margin that should be different in the rifted part and in the undeformed part of the margin. The style of elastic deformation will be a function of the elastic thickness, *Te*. During the first 20 Ma of the post-breakup history, *Te* of the stretched margin is low compared to that of the continent; leading to elastic deformation with low wavelengths while in the continent, larger wavelengths should dominate. The opposite is expected for time larger than 20 Ma. Further numerical models are required to quantify these effects.

Fig. 8 presents a synthetic view of the time evolution of the topography, temperature, strength, and deformation of the two types of margins. In early stages (phase 1, between 0 and ∼80 Ma), thermal subsidence and thermal uplift occurs in the stretched and unstretched part of the margins, respectively, because of thermal re-adjustment and lateral heating. Consequently, the vertical load applied to the margin drastically changes along the margin from a downward load in the stretched part to a upward load in the unstretched part. This large difference will increase with time and could trigger flexure of the margin. Flexural deformation of the margin could enhance subsidence and uplift. Flexural response will be maximum in the less resistant part of the margin that is at that time the stretched part. The differential applied load is maximum for volcanic margin, and thus flexure and uplift enhancement is expected to be maximum for the volcanic margin. The timing of these processes is faster for volcanic margin. In later stages (phase 2, after 80 Ma, Fig. 8) the entire margin undergoes subsidence that explains the decrease of the topography in the unstretched part of the margin where uplift previously prevailed. Lateral differences in vertical load applied to the margin still exist because of the non-horizontality of the base of the lithosphere. However, these lateral variations in applied load are significantly less than that of early stage. Consequently, the flexural response of the margin will be less favoured, and uplift and subsidence less enhanced. At these times, the unstretched part of the margin becomes the less resistant part of the margin. An applied horizontal stress (far field stresses like ridge-push) would induce an important deformation in this part of the margin and thus explain a possible tectonic uplift at these times. 2-D modelling that will combine thermal, strength and flexural evolution of the margin would be now crucial to accurately understand margin topography. The present 2-D thermal modelling should be seen here as primary models to document the impact of lateral variations in temperature and strength through time during the post-breakup evolution of a passive margin.

5 CONCLUSION

A 2-D finite element numerical model was performed to evaluate the vertical and horizontal conductive thermal evolution of continental passive margins, from the breakup to the late thermal equilibrium, and its role on the post-rift topography of volcanic and non-volcanic passive margins. The main results are:

1. The thermal evolution occurs in two phases. The first phase occurs between 0 and 80 Ma after the breakup and is characterized by a thermal thinning of the unstretched lithosphere, and by a thermal thickening in the stretched continental lithosphere. The second phase occurs after 80 Ma and is characterized by the thickening of the continental lithosphere in both zones.

2. Thermal thickening and thermal thinning lead to subsidence and uplift, respectively. The thermal uplift induced by isostatic movements is up to 250 m in the landward part of the volcanic

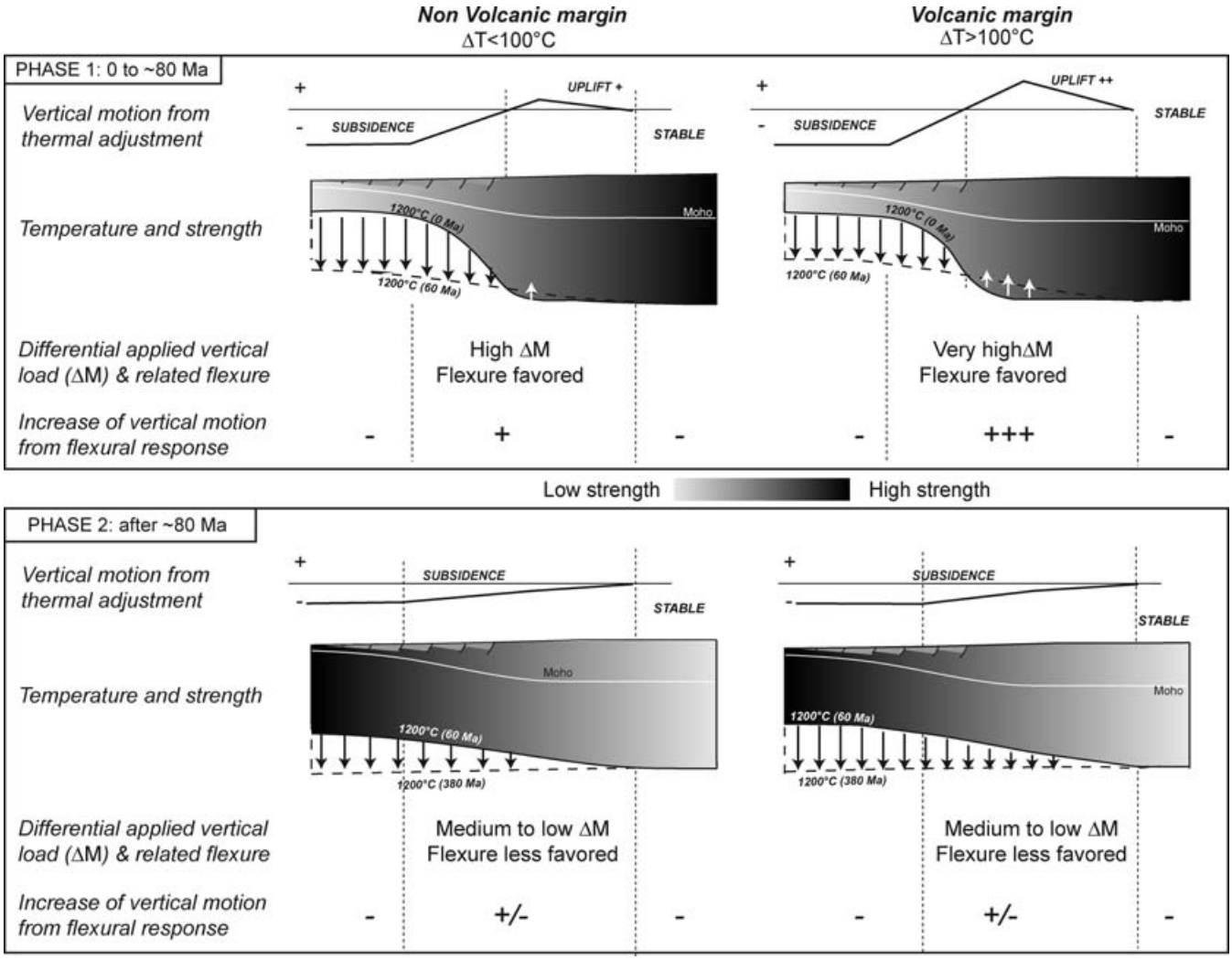

Figure 8. Schematic drawing of the time evolution of the vertical motion of the margin inferred by 2-D thermal re-adjustments. The strength evolution, the flexural response and subsequent increase in vertical motion of the margin are also reported for the two stages of the margin evolution.

margins and is about twice the computed uplift for non-volcanic margins.

3. The numerical results are qualitatively consistent with the topographic observations of passive margins in nature. The volcanic passive margins are indeed two to three times higher than non-volcanic margins but both margins are three to four times more elevated in nature than in the model predictions. The thermal conduction contribution to the uplift may be small (10–25 per cent) and others deformation mechanisms, such as flexure, small-scale convection and tectonic movements, should play an important role in vertical movements.

4. The inferred time evolution of the margin topography are consistent with natural data. We have inferred maximum relief of the margin after 40–80 Ma after the breakup and then a linear decrease of the margin topography with time.

5. The stretched part of the continental margin is weaker than the undeformed continent just after the breakup and progressively becomes stronger than the undeformed continent. The elastic thickness and the strength of the stretched margin becomes larger than the elastic thickness and the strength of the undeformed continent after 20 and 80 Ma, respectively. This strength inversion during the post-breakup history of the passive margin should have major impacts in terms of vertical movements of the margin and more generally in terms of style of deformation.

ACKNOWLEDGMENTS

We thank R. Huismans and an anonymous reviewer for their comments on a previous version of this manuscript. Fruitful discussions with Michel Rabinowicz help us to improve this manuscript. Groupement de Recherche 'GDR Marges – volet Marges Anciennes', funded this work.

REFERENCES

Banda, E., Gallart, J., Garcia-Duenas, V., Danobeitia, J.J. & Makris, J., 1993. Lateral variation of the crust in the Iberian peninsula: new evidence from the Betic Cordillera, *Tectonophysics,* **221,** 53–66.

Bauer, K. *et al.*, 2000. Deep structure of the Namibia continental margin as derived from integrated geophysical studies, *J. geophys. Res.,* **105**(B11), 25 829–25 853.

Beaumont, C., Keen, C.E. & Boutillier, R., 1982. Comparison of foreland and Atlantic type basins, *Phil. Trans. Roy. Soc. Lond.* A, **305,** 295–317.

Beaumont, C., Kooi, H. & Willett, S., 2000. Coupled tectonic-surface process models with applications to rifted margins and collisional orogens, in *Geomorphology and Global Tectonics,* pp. 29–55, ed. Summerfield, M.A., John Wiley & Sons, Chichester.

Boillot, G., 1979. *Géologie des Marges Continentales,* 139 pp, Masson, Paris.

Boldreel, L.O. & Andersen, M.S., 1998. Tertiary compressional structures on the Faroe-Rockall Plateau in relation to northeast Atlantic ridge-push and Alpine foreland stresses, *Tectonophysics,* **300,** 13–28.

Bott, M.P.H., 1996. Flexure associated with planar faulting, *Geophys. J. Int.,* **126,** F21–F24.

Boutilier, R.R. & Keen, C.E., 1999. Small-scale convection and divergent plate boundaries, *J. geophys. Res.,* **104**(B4), 7389–7403.

Braun, J. & Beaumont, C., 1989. A physical explanation of the relation between flank uplifts and the breakup unconformity at rifted continental margins, *Geology,* **17,** 760–764.

Brun, J.P., 1999. Narrow rifts versus wide rifts: inferences for the mechanics of rifting from laboratory experiments, *Phil. Trans. Roy. Soc. Lond.,* **357,** 695–712.

Buck, W.R., 1986. Small-scale convection induced by passive rifting: the cause for uplift of rift shoulders, *Earth Planet. Sci. Lett.,* **77,** 362–372.

Burke, K., 1996. The African Plate, *South African J. Geol.,* **99**(4), 341–409.

Burov, E. & Poliakov, A., 2001. Erosion and rheology controls on synrift and postrift evolution: verifying old and new ideas using a fully coupled numerical model, *J. geophys. Res.,* **106**(B8), 16 461–16 481.

Burov, E. & Watts, A.B., 2006. The long-term strength of continental lithosphere: "jelly sandwich" or "crème brûlée"?, *GSA Today,* **16**, 1.

Chéry, J., Lucazeau, F., Daignières, M. & Vilotte, J.P., 1992. Large uplift of rift flanks: a genetic link with lithospheric rigidity, *Earth Planet. Sci. Lett.,* **112**(1–4), 195–211.

Clift, P., 1996. Plume tectonics as a cause of mass wasting on the southeast Greenland continental margin, *Marine Petrol. Geol.,* **13**(7), 771–780.

Clift, P.D., 1997. Temperature anomalies under the Northeast Atlantic rifted volcanic margins, *Earth Planet. Sci. Lett.,* **146,** 195–211.

Cloetingh, S., Gradstein, F.M., Kooi, H., Grant, A.C. & Kaminski, M., 1990. Plate reorganisation: a cause of rapid late Neogene subsidence and sedimentation around the North Atlantic?, *J. Geol. Soc. Lond.,* **147,** 495–506.

Cobbold, P.R., Meisling, K.E. & Mount, S.V., 2001. Reactivation of an obliquely-rifted margin. Campos and Santos basins, SE Brazil, *Am. Assoc. Petr. Geol.,* **85**(11), 1925–1944.

Cochran, J.R., 1983. Effects of finite rifting times on the development of sedimentary basins, *Earth Planet. Sci. Lett.,* **66,** 289–302.

Coffin, M.F. & Eldholm, O., 1992. Volcanism and continental break-up: a global compilation of large igneous provinces, in *Magmatism and the Causes of Continental Break-Up,* pp. 17–30, eds Storey, B.C., Alabaster, T. & Pankhurst, R.J., Geological Society Special Publications, London.

Doré, A.G. & Lundin, E.R., 1996. Cenozoic compressional structures on the NE Atlantic margin: nature, origin and potential significance for hydrocarbon exploration, *Petrol. Geosci.,* **2,** 299–311.

Eldholm, O., 1991. Magmatic-tectonic evolutions of a volcanic rifted margin, *Marine Geol.,* **102,** 43–61.

Eldholm, O., Gladczenko, T.P., Skogseid, J. & Planke, S., 2000. Atlantic volcanic margins: a comparative study, in *Dynamics of the Norwegian Margin,* pp. 411–428, ed. Nottvedt, A., Geological Society of London Special Publications, London.

Emery, K.O. & E. Uchupi, 1984, *The Geology of the Atlantic Ocean,* 1050 pp., Springer Verlag, Berlin.

Fjeldskaar, W., Lindholm, C., Dehls, J.F. & Fjeldskaar, I., 2000. Postglacial uplift, neotectonics and seismicity in Fennoscandia, *Quater. Sci. Rev.,* **19,** 1413–1422.

Gadd, S.A. & Scrutton, R.A., 1997. An integrated thermomechanical model for transform continental evolution, *Geo-Marine Lett.,* **17,** 21–30.

Gallagher, K. & Brown, R., 1999. The mesozoic denudation history of the Atlantic margins of southern Africa and southeast Brazil and the relationship to offshore sedimentation, in *The Oil and Gas Habitats of the South Atlantic,* pp. 41–53, eds Cameron, N.R., Bate, R.H., & Clure, V.S., Geological Society of London Special Publications, London.

Geoffroy, L., 2001. The structure of volcanic margins: some problematics from the North-Atlantic/Labrador-Baffin system, *Marine Petrol. Geol.,* **18,** 463–469.

Gilchrist, A.R. & Summerfield, M.A., 1990. Differential denudation and flexural isostasy in formation of rifted-margin upwarps, *Nature,* **346,** 739–742.

Gilchrist, A.R., Kooi, H. & Beaumont, C., 1994. Post-Gondwana geomorphic evolution of southwestern Africa: implications for the controls on landscape development from observations and numerical experiments, *J. geophys. Res.,* **99**(B6), 12 211–12 228.

Gladczenko, T.P., Hinz, K., Eldholm, O., Meyer, H., Neben S. & Skogseid, J., 1997. South-Atlantic volcanic margins, *J. Geol. Soc. Lond.,* **154,** 465–470.

Gunnel, Y. & Fleitout, L., 2000. Morphotectonic evolution of the Western Ghats India, in *Geomorphology and Global Tectonics,* pp. 89–121, ed. Summerfield, M.A., John Wiley & Sons, Chichester.

Gurnis, M., Mitrovica, J.X., Ritsema, J. & Heijst, H.J.V., 2000. Constraining mantle density structure using geological evidence of surface uplift rates: the case of the African Superplume, *Geochem., Geophys., Geosys.,* **1**, doi:1999GC000035.

Hansen, D.L. & Nielsen, S.B., 2002. Does thermal weakening explain basin inversion? Stochastic modelling of the thermal structure beneath sedimentary basins, *Earth Planet. Sci. Lett.,* **198,** 113–127.

Hopper, J.R. & Buck, W.R., 1996. The effect of lower crustal flow on continental extension and passive margin formation. *J. Geophys. Res. – Solid Earth,* **101**(A10), 21–795, doi:96JB01644.

Hopper, J.R. & Buck, W.R., 1998. Styles of extensional decoupling. *Geology,* **26**(8), 699–702.

Hudec, M.R. & Jackson, M.P.A., 2002. Structural segmentation, inversion, and salt tectonics on a passive margin: evolution of the Inner Kwanza Basin, Angola, *Geol. Soc. Am. Bull.,* **114**(10), 1222–1244.

Huismans, R.S., Podladchikov, Y.Y. & Cloetingh, S., 2001. Transition from passive to active rifting: relative importance of asthenospheric doming and passive extension of the lithosphere, *J. geophys. Res.,* **106**(B6), 11 271–11 291.

Jackson, M.P.A., Cramez, C. & Fonck, J.M., 2000. Role of subaerial volcanic rocks and mantle plumes in creation of South Atlantic margins: implications for salt tectonics and source rocks, *Marine Petrol. Geol.,* **17,** 477–498.

Japsen, P. & Chalmers, J.A., 2000. Neogene uplift and tectonics around the North Atlantic: overview, *Global Planet. Change,* **24,** 165–173.

Karato, S.-I. & Wu, P., 1993. Rheology of the upper mantle: a synthesis. *Science,* **260,** 771–778.

Karner, G.D., 1985. Thermally induced residual topography within oceanic lithospere. *Nature,* **318,** 527–532.

Keen, C.E. & Boutillier, R.R., 2000. Interaction of rifting and hot horizontal plume sheets at volcanic margins. *J. geophys. Res.,* **105**(B6), 13 375–13 387.

King, S.D. & Anderson, D.L., 1998. Edge-driven convection, *Earth Planet. Sci. Lett.,* **160,** 289–296.

Kruse, S., McNutt, M., Phipps-Morgan, J. & Royden, L., 1991. Lithospheric extension near Lake Mead, Nevada – a model for ductile flow in the lower crust, *J. geophys. Res.,* **96,** 4435–4456.

Leroy, M., Dauteuil, O. & Cobbold, P. 2004. Compression of passive margins: controls from oceanic lithosphere rheology, *Geophys. J. Int.,* **159,** 400–411.

McKenzie, D., 1978. Some remarks on the development of sedimentary basins, *Earth Planet. Sci. Lett.,* **40,** 25–32.

Menzies, M.A., Klemperer, S.I., Ebinger, C.J. & Baker, J., 2002. Characteristics of volcanic rifted margins, *Geol. Soc. Am. Special paper*, pp. 14.

Mohriak, W.U. & Dewey, J.F., 1987. Deep seismic reflectors in the Campos basin, offshore Brazil, *Geophys. J. Roy. Astronom. Soc.,* **89**(1), 133–140.

Mosar, J., Lewis, G. & Torsvik, T.H., 2002. North Atlantic sea-floor spreading rates: implications for the Tertiary development of inversion structures of the Norwegian-Greenland Sea, *J. Geol. Soc. Lond.,* **159,** 503–515.

Nielsen, T.K. & Hopper, J.R., 2002. Formation of volcanic rifted margins: are temperatures anomalies required? *Geophys. Res. Lett.,* **29**(21), 2002, doi:10.1029/2002GL015681.

Nyblade, A.A. & Robinson, S.W., 1994. The African superswell, *Geophys. Res. Lett.,* **21**(9), 765–768.

Parsons, B. & Sclater, J.G., 1977. An analysis of the variation of ocean floor bathymetry and heat flow with age. *J. geophys. Res.,* **82,** 803–827.

Partridge, T.C. & Maud, R.R., 1987. Geomorphic evolution of southern Africa since the Mesozoic, *South African J. Geol.,* **90**(2), 179–208.

Pinet, C., Jaupart, C., Mareschal, J.C., Gariepy, C., Benfait, G. & Lapointe, R., 1991. Heat flow and structure of the lithosphere in the eastern Canadian Shield, *J. geophys. Res.,* **96,** 19 941–19 963.

Price, S., Brodie, J., Whitham, A. & Kent, R., 1997. Mid-Tertiary rifting and magmatism in the Traill Ø region, East Greenland, *J. Geol. Soc. Lond.,* **154,** 419–434.

Ranalli, G., 1995. *Rheology of the Earth*. Chapman & Hall, London.

Ransome, I.G.D. & de Wit, M.J., 1992. Preliminary investigations into a microplate model for the South Western Cape, in *Inversion Tectonics of the Cape Fold Belt, Karoo and Cretaceous Basins of Southern Africa,* pp. 257–267, eds de Wit, M.J. & Ransome, I.G.D., Balkema, Rotterdam, Holland.

Rowley, D.B. & Sahagian, D., 1986. Depth-dependent stretching: a different approach. *Geology,* **14,** 32–35.

Ruppel, C., 1995. Extensional processes in continental lithosphere, *J. geophys. Res.,* **100,** 24 187–24 215.

Saenz, C.A.T., Hackspacher, P. C., Neto, J.C.H., Iunes, P.J., Guedes, S., Ribeiro, L.F.B. & Paulo, S.R., 2003. Recognition of cretaceous, paleocene, and neogene tectonic reactivation through apatite fission-track analysis in Precambrian areas of southeast Brazil: association with the opening of the South-Atlantic Ocean, *J. South Am. Earth Sci.,* **15**(7), 765–774.

SARPP, 2003. *Structural Analysis and Rock Physics Program,* LMS, Ecole Polytechnique, Palaiseau, France.

Skogseid, J., 2001. Volcanic margins: geodynamic and exploration aspects, *Marine Petrol. Geol.,* **18,** 457–461.

Skogseid, J., Pedersen, T., Eldholm, O. & Larsen, B.T., 1992. Tectonism and magmatism during NE Atlantic continental break-up: the Vøring Margin, in *Magmatism and the Causes of Continental Break-Up,* pp. 305–320, eds Storey, B.C., Alabaster, T. & Pankhurst, R.J., Geological Society of London Special Publication, London.

Stein, C.A. & Stein, S., 1992. A model for the global variation in oceanic depth and heat flow with lithospheric age, *Nature,* **359,** 123–129.

Stuevold, L.M. & Eldholm, O., 1996. Cenozoic uplift of Fennoscandia inferred from a study of the mid-Norwegian margin, *Global Planet. Changes,* **12,** 359–386.

Vagnes, E., 1997. Uplift at thermo-mechanically coupled ocean-continent transforms: modeled at the Senja Fracture Zone, southwestern Barents Sea, *Geo-Marine Lett.,* **17,** 100–109.

Van Der Beek, P., Andriessen, P. & Cloetingh, S., 1995. Morphotectonicevolution of rifted continental margins: inferences from a coupled tectonic-surface processes model and fission track thermochronology, *Tectonics,* **14,** 406–421.

Van Wijk, J.W., Huismans, R.S., ter Voorde, M. & Cloetingh, S.A.P.L., 2001. Melt generation at volcanic continental margins: no need for a mantle plume? *Geophys. Res. Lett.,* **28**(20), 3995–3998.

Watts, A.B. & Ryan, W.B.F., 1976. Flexure of the lithosphere and continental margin basins, *Tectonophysics,* **36,** 25–44.

Weissel, J.K. & Karner, G.D., 1989. Flexural uplift of rift flanks due to mechanical unloading of the lithosphere during extension. *J. geophys. Res.,* **94**(B10), 13 919–13 950.

White, R. & McKenzie, D., 1989. Magmatism at rift zones: the generation of volcanic continental margins, *J. geophys. Res.,* **94**(B6), 7685–7729.